American Mineralogist, Volume 97, pages 573–582, 2012

Compressibility and thermal expansion of hydrous ringwoodite with 2.5(3) wt% H_2O

Yu Ye,[1,*] David A. Brown,[2] Joseph R. Smyth,[2] Wendy R. Panero,[3] Steven D. Jacobsen,[4] Yun-Yuan Chang,[4] Joshua P. Townsend,[4] Sylvia-Monique Thomas,[4,†] Erik H. Hauri,[5] Przemyslaw Dera,[6] and Daniel J. Frost[7]

[1]Department of Physics, University of Colorado at Boulder, Boulder, Colorado 80309, U.S.A.
[2]Department of Geological Sciences, University of Colorado at Boulder, Boulder, Colorado 80309, U.S.A.
[3]School of Earth Sciences, Ohio State University, Columbus, Ohio 43210, U.S.A.
[4]Department of Earth and Planetary Sciences, Northwestern University, Evanston, Illinois 60208, U.S.A.
[5]Department of Terrestrial Magnetism, Carnegie Institution of Washington, 5241 Broad Branch Road NW, Washington, D.C. 20015, U.S.A.
[6]Center for Advanced Radiation Sources, University of Chicago, Argonne National Laboratory, Argonne, Illinois 60439, U.S.A.
[7]Bayerisches Geoinstitut, Universität Bayreuth, D95440 Bayreuth, Germany

Abstract

Ringwoodite (γ-Mg_2SiO_4) is the stable polymorph of olivine in the transition zone between 525–660 km depth, and can incorporate weight percent amounts of H_2O as hydroxyl, with charge compensated mainly by Mg vacancies ($Mg^{2+} = 2H^+$), but also possibly as ($Si^{4+} = 4H^+$ and $Mg^{2+} + 2H^+ = Si^{4+}$). We synthesized pure Mg ringwoodite containing 2.5(3) wt% H_2O, measured by secondary ion mass spectrometry (SIMS), and determined its compressibility at 300 K by single-crystal and powder X-ray diffraction (XRD), as well as its thermal expansion behavior between 140 and 740 K at room pressure. A third-order Birch-Murnaghan equation of state (BM3 EOS) fits values of the isothermal bulk modulus $K_{T0} = 159(7)$ GPa and $(dK_T/dP)_{P=0} = K' = 6.7(7)$ for single-crystal XRD; $K_{T0} = 161(4)$ GPa and $K' = 5.4(6)$ for powder XRD, with $K_{T0} = 160(2)$ GPa and $K' = 6.2(3)$ for the combined data sets. At room pressure, hydrous ringwoodite breaks down by an irreversible unit-cell expansion above 586 K, which may be related to dehydration and changes in the disorder mechanisms. Single-crystal intensity data were collected at various temperatures up to 736 K, and show that the cell volume V(cell) has a mean thermal expansion coefficient α_{V0} of $40(4) \times 10^{-6}$/K (143–736 K), and $29(2) \times 10^{-6}$/K (143–586 K before irreversible expansion). V(Mg) have α_0 values of $41(3) \times 10^{-6}$/K (143–736 K), and V(Si) has α_0 values of $20(3) \times 10^{-6}$/K (143–586 K) and $132(4) \times 10^{-6}$K (586–736 K). Based on the experimental data and previous work from ^{29}Si NMR, we propose that during the irreversible expansion, a small amount of H^+ cations in Mg sites transfer to Si sites without changing the cubic spinel structure of ringwoodite, and the substituted Si^{4+} cations move to the normally vacant octahedral site at (½, ½, 0). Including new SIMS data on this and several Mg-ringwoodite samples from previous studies, we summarize volume-hydration data and show that the $Mg^{2+} = 2H^+$ dominates up to about 2 wt% H_2O, where a discontinuity in the volume vs. H_2O content trend suggests that other hydration mechanisms become important at very high H_2O contents.

Keywords: Compressibility, hydrous ringwoodite, irreversible thermal expansion

Introduction

For a pyrolite-model upper mantle composition (Anderson 2007; Ringwood 1966), ringwoodite-$(Mg,Fe)_2SiO_4$ dominates the mineralogy of the lower transition zone from 525 to 660 km depth. At 525 km depth, wadsleyite transforms to ringwoodite at about 1790 K, whereas at 660 km depth, ringwoodite breaks down into perovskite plus ferropericlase (Mg,Fe)O at about 1873 K (e.g., Ito and Katsura 1989). Ringwoodite has the cubic spinel structure ($Fd\bar{3}m$), with Mg in the octahedral site (½, ½, ½), and Si in the tetrahedral site (1/8, 1/8, 1/8), with little or no site disorder at 300 K as supported by the ^{29}Si NMR study of Stebbins et al. (2009a). The most hydrous ringwoodite could contain up to about 3 wt% H_2O (e.g., Kohlstedt et al. 1996), and a ^{29}Si NMR spectroscopic study by Stebbins et al. (2009b) demonstrated that most H^+ substitution occurs at the Mg site, whereas the presence of short Si-H distance indicated a significant, although minor amount of Si-OH (silanol) groups.

Hydration increases the molar volume of ringwoodite (e.g., Inoue et al. 1998; Smyth et al. 2003) and therefore also its thermal expansivity (Ye et al. 2009) and compressibility (e.g., Yusa et al. 2000; Smyth et al. 2004), and significantly reduces its elastic moduli (e.g., Inoue et al. 1998; Wang et al. 2003, 2006; Jacobsen et al. 2004; Jacobsen and Smyth 2006). However, the relationship between H_2O content and its influence on various physical properties important to geophysical research relies on precise determination of H_2O concentrations in the crystal lattice, which have suffered from the absence of an absolute spectroscopic calibration for water content. The increasing amount of SIMS data for Mg-ringwoodite samples justifies an updated

* E-mail: yey@colorado.edu
† Present Address: Department of Geoscience, University of Nevada Las Vegas, Las Vegas, Nevada 89154, U.S.A.

0003-004X/12/0004–573$05.00/DOI: http://dx.doi.org/10.2138/am.2012.4010

compilation following Smyth et al. (2003) of systematic lattice hydration data presented here.

Manghnani et al. (2005) reported the compressibility of hydrous iron-bearing ringwoodite (0.79 wt% H_2O) by powder XRD in the diamond-anvil cell up to 45 GPa at room temperature and observed no phase changes. Yusa et al. (2000) carried out a high-pressure study of hydrous pure-Mg ringwoodite (2.8 wt% H_2O) up to 6 GPa. In addition, Smyth et al. (2004) and Ganskow et al. (2010) also presented isothermal compressibility studies for hydrous iron-bearing ringwoodite samples (less than 1 wt% H_2O). Elasticity studies at pressures were reported for both anhydrous ringwoodite (Sinogeikin et al. 2003; Li 2003) and hydrous ringwoodite (Jacobsen et al. 2004; Jacobsen and Smyth 2006; Wang et al. 2006). These studies consistently report that hydration significantly decreases both isothermal and adiabatic bulk moduli, but increases K'. For our current sample with up to 2.5(3) wt% H_2O, high-pressure experiments of both single-crystal and powder XRD were conducted, and the compressibility results are compared with literature values, and the effect of hydration on density and seismic velocities are evaluated.

In addition to nano-SIMS data on the current sample containing 2.5(3) wt% H_2O, we report new SIMS data for two previous samples (ringby2 and ringby4) from the study of Smyth et al. (2003), containing 0.8(2) and 0.16(5) wt% H_2O, respectively. Analysis of these data along with other studies using SIMS water contents, we construct a volume-hydration data set wherein up to about 2 wt% the $Mg^{2+} = 2H^+$ substitution mechanism is dominant. A discontinuity in the volume-hydration curve at about 2 wt% suggests that at higher water content, the $Si^{4+} = 4H^+$ and possibly $Mg^{2+} + 2H^+ = Si^{4+}$ become important.

Ye et al. (2009) reported a disequilibrium irreversible expansion for this hydrous ringwoodite sample starting at 606 K, which is different from observation that hydrous ringwoodite powder begins to dehydrate at 723 K (Inoue et al. 2004). This irreversible expansion affects unit-cell volumes measured at ambient conditions after heating. To understand the internal structure change during irreversible expansion observed in hydrous samples, we have conducted intensity scans and refined structure parameters for hydrous ringwoodite.

Experiments

Sample synthesis and characterization

The sample of hydrous ringwoodite was synthesized using the 5000-ton press at Bayerisches Geoinstitut, Universität Bayreuth, Germany (sample SZ0820; BGI run no. Z636). A 2 mm welded Pt capsule with 0.2 mm wall thickness was used in an 18/8 assembly (18 mm MgO octahedron compressed using carbide anvils with 8 mm corner truncations). The synthesis conditions were 20 GPa and 1523 K with a heating duration of 3.5 h. The starting material was synthetic forsterite with added brucite and silica (quartz) to make a composition with about 2.8 wt% H_2O. Only ringwoodite was identified in the synthesized material.

A single crystal of the material designated as SZ0820T approximately 100 µm in average dimension was selected for room *P-T* XRD, Raman, Fourier transform infrared spectroscopy (FTIR), and nano-SIMS measurements. The unit-cell volume from single-crystal XRD of SZ0820T was $V_0 = 527.97(7)$ Å^3. Raman and FTIR spectra of sample SZ0820T are shown in Figure 1 for characterization purposes. Whereas the water content of ringwoodite SZ0820T from FTIR using the calibration of Libowitzky and Rossman (1997) gives 1.6 wt% H_2O, using a molar absorption coefficient of 100 000 L/[mol(H_2O)·cm^2] determined by Koch-Müller and Rhede (2010), we obtain a value of 2.3 wt% H_2O, which is in good agreement with estimates of 2.5(6) wt% H_2O from the lattice parameter (Smyth et al. 2003).

The same crystal (SZ0820T) was analyzed on the Cameca NanoSIMS 50L at the Department of Terrestrial Magnetism, Carnegie Institute of Washington. SIMS measurements were made with a 1 nA Cs+ primary beam sputtering a crater 7 × 7 µm^2, and beam blanking was employed to restrict the data collection from the central 2.6 × 2.6 µm area in the center of the sputtered crater. In SZ0820T, seven different probe points from rim-to-rim gave an average water content of 2.66(4) wt% H_2O. Two spots with anomalously high water content of ~3 wt% coincided with cracks in the crystal, and from the remaining five points we obtain an average value of 2.5(3) wt% H_2O, used in this study. In addition to SZ0820, we also measured two other hydrous Mg-ringwoodite crystals (from a previous study) at DTM on the 6F SIMS instrument; ringby 2 and ringby4 from the study of Smyth et al. (2004). A crystal from each of those runs was analyzed and from two data points each we obtained a water content of 0.16(5) wt% H_2O for ringby4 and for ringby2 we obtained a water content of 0.76(20) wt% H_2O.

The volumes of hydration of Mg-ringwoodites are summarized in Table 1 and Figure 2. Table 1 includes SIMS water content data exclusively, and also only single-crystal volume-hydration data (with the exception of Yusa et al. 2000) as discussed in the following section. Using only carefully selected single-crystal data and SIMS water contents, we produce a systematic data set from which to study the change in volume (Fig. 2), Mg/Si (Fig. 3), and density (Fig. 4) of ringwoodite. The numbered data points correspond to references numbered in Table 1. CIF files available on deposit.[1]

High-pressure single-crystal and powder XRD

High-pressure single-crystal XRD measurements for this sample were carried out at GSECARS beamline 13 BM-D, Advanced Photon Source (APS), Argonne National Laboratory. The size of the single crystal for the high-pressure measurement was about 45 × 40 × 30 µm^3. We used a symmetric piston-cylinder type diamond-anvil cell (DAC) with 300 µm culets and a rhenium gasket pre-indented to 50 µm, with a 150 µm diameter hole drilled through the center. The

[1] Deposit item AM-12-030, CIFs. Deposit items are available two ways: For a paper copy contact the Business Office of the Mineralogical Society of America (see inside front cover of recent issue) for price information. For an electronic copy visit the MSA web site at http://www.minsocam.org, go to the *American Mineralogist* Contents, find the table of contents for the specific volume/issue wanted, and then click on the deposit link there.

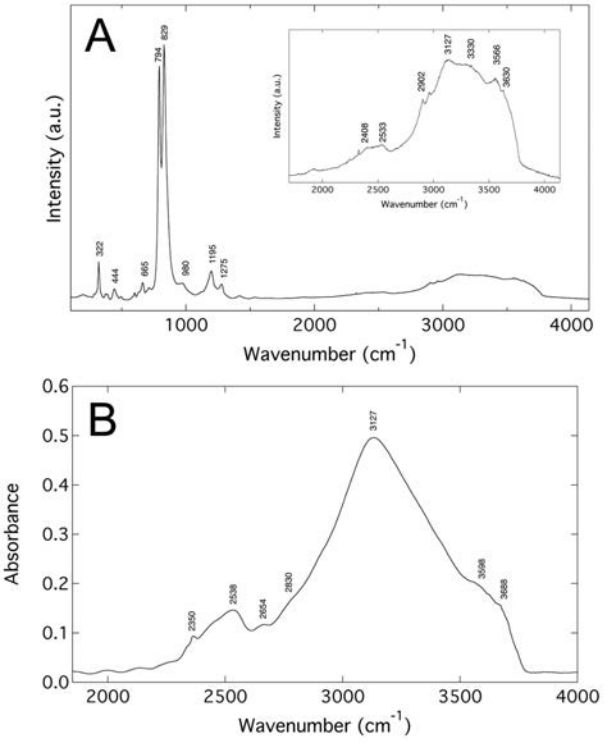

Figure 1. (**a**) Raman and (**b**) FTIR spectra of ringwoodite crystal SZ0820T used in the current study.

TABLE 1. Lattice hydration data for Mg-ringwoodite samples, including H_2O contents from SIMS measurements, Mg/Si ratios from microprobe analyses, and unit-cell volumes from X-ray diffraction

wt% H_2O	Mg/Si	H pfu†	V_0 (Å^3)	ρ_0 (g/cm^3)	Reference
0	2.00	0.000	524.56	3.563	(1)‡ Sasaki et al. (1982)
0.16(5)*	1.98	0.025	524.25(7)	3.558	(2) Smyth et al. (2003) Sample ringby4
0.200(4)	1.97	0.031	524.60(10)	3.552	(3) Kudoh et al. (2007)
0.76(20)*	1.96	0.118	525.21(11)	3.527	(4) Smyth et al. (2003) Sample ringby2
2.0(2)	1.94	0.306	526.41(9)	3.476	(5) Kudoh et al. (2000)
2.2(2)	1.95	0.336	527.24(3)	3.466	(6) Inoue et al. (1998)
2.3(1)	1.88	0.356	530.10(1.2)	3.434	(7) Wang et al. (2006)
2.5(3)*	1.90§	0.380	527.97(7)	3.445	(8) This study Sample SZ0820
2.8(2)	1.88	0.424	529.14(24)	3.425	(9) Yusa et al. (2000)

* These SIMS water contents determined in this study.
† Hydrogen atoms per formula unit: calculated assuming $Mg^{2+} = 2H^+$, balanced by $Si^{4+} = 4H^+$ or $Mg^{2+} + 2H^+ = Si^{4+}$.
‡ Numbers in parentheses refer to data points plotted in Figures 2–4.
§ Determined from the trend in Figure 2.

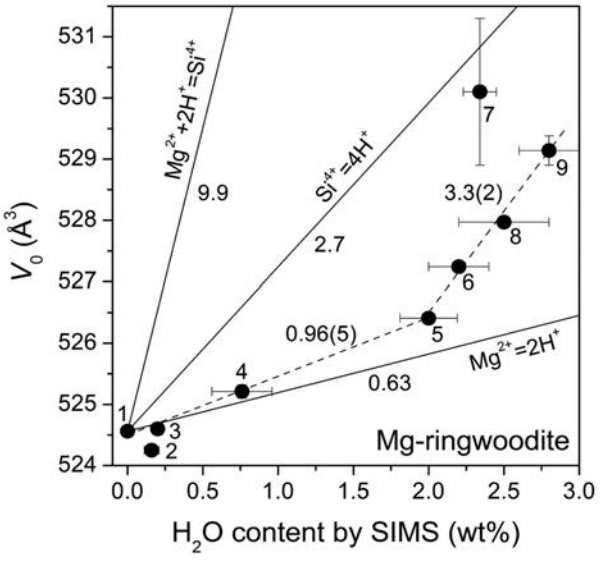

FIGURE 2. Volume of Mg-ringwoodite crystals as a function of water content determined by SIMS. Numbered data points correspond to references in Table 1. (Point 8 is for the current study, and the points in Figs. 3 and 4 are numbered in the same order.) Fitted curves to the data below and above 2 wt% H_2O are shown by dashed lines with slopes 0.96(5) and 3.3(2), respectively. Solid lines show predicted volume trends for various hydration mechanism calculated by LDA from Panero (2010).

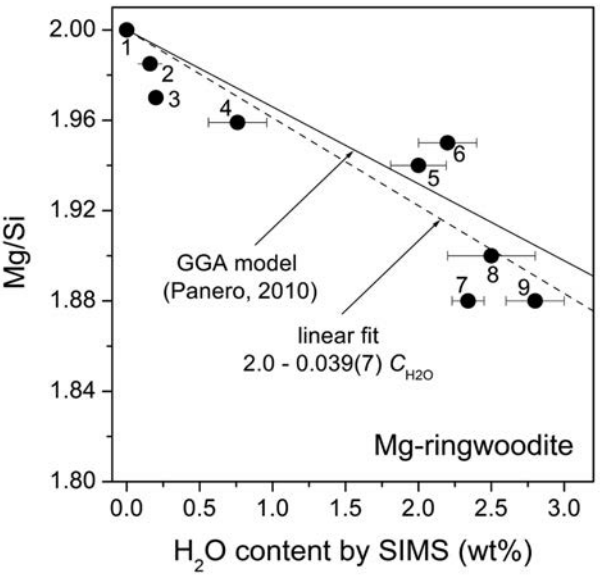

FIGURE 3. Plot of the Mg/Si ratio (from microprobe analysis) against SIMS water contents from the data presented Table 1.

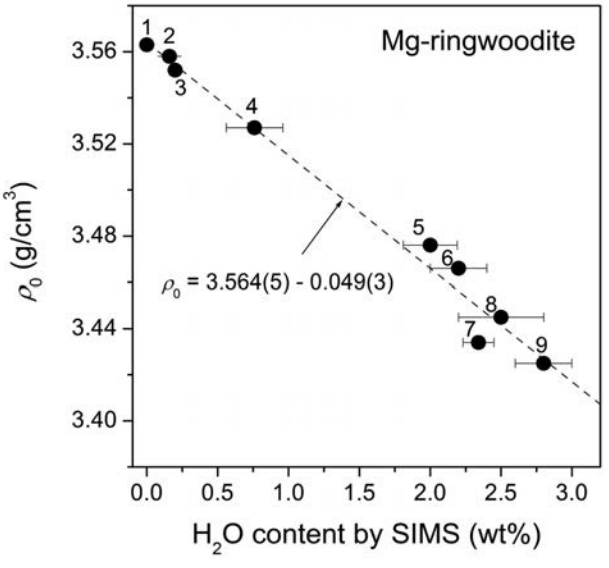

FIGURE 4. Variation of density (ρ_0) with water content from the references presented in Table 1.

DAC was loaded with neon as pressure medium using the COMPRES/GSECARS gas-loading system (Rivers et al. 2008). The initial pressure inside the cell was about 1.28 GPa after closing DAC, with the gasket-hole diameter shrunk by about one-third. Monochromatic synchrotron radiation (λ = 0.3344 Å) was used to collect diffraction patterns on a MAR345 image plate. The single-crystal diffraction data collection at each pressure took 6 to 8 min with omega rotation from +25° to –25°. To obtain the orientation matrix at the initial pressure of 1.3 GPa, an omega step-scan was performed with a rotation of 1° per minute for one image. In total, 50 images were collected to calculate omega angles for each reflection and the orientation matrix, as well as unit-cell parameters. This orientation matrix was used as a first approximation to index peaks in images collected at subsequent pressures. An annealed ruby sphere placed in the sample chamber along with the sample served as pressure marker. Pressure was determined by the shift of R1 fluorescence (Mao et al. 1986). The crystal fractured between the two diamond-anvils at about 29 GPa.

The diffraction patterns at 1.3 GPa, 6.7 GPa, 11.2 GPa, and 14.8 GPa are shown in Figures 5a–5d, created with software package GSE-ADA (Dera 2007a). Reflections from single-crystal hydrous ringwoodite appear as sharp spots in the diffraction patterns. Reflections of neon appear at the pressure step of 6.7 GPa and above, and occur as sharp spots at 6.7 and 8.9 GPa, and as short "streaks" at pressures above 8.9 GPa. For steps above 6 GPa, pressure was calculated from neon reflections by the equation of states from Fei et al. (2007) and Dorogokupets and Dewaele (2007). For each step, at least 30 reflection spots from hydrous ringwoodite were used to refine the unit-cell parameters using software packages GSE-ADA (Dera 2007a) and RSV (Dera 2007b). Both the pressure values from ruby and neon are listed in Table 2, as well as the unit-cell parameters of

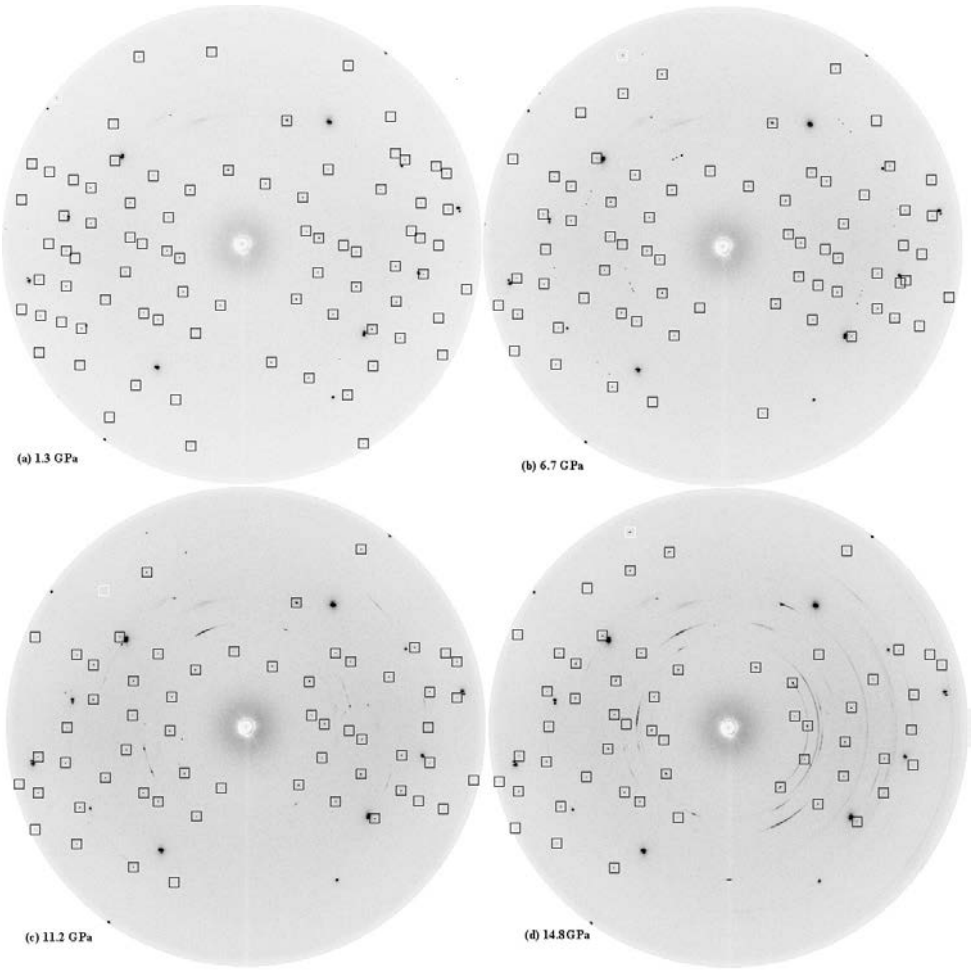

FIGURE 5. Parts **a**–**d** are the reflection patterns at 1.3, 6.7, 11.2, and 14.8 GPa, respectively. The reflection "spots" from single crystal of hydrous ringwoodite are marked in boxes, while the unmarked but very strong "spots" are from diamond reflections. Neon reflections could be clearly identified as "streaks" in the patterns at 11.2 and 14.8 GPa.

TABLE 2. Unit-cell parameters vs. pressure for single-crystal XRD

P_{ruby} (GPa)	P_{neon} (GPa)	a (Å)	V (Å^3)
1.3(1)	–	8.068(3)	525.1(3)
2.7(1)	–	8.049(3)	521.4(3)
4.5(1)	–	8.021(3)	516.1(3)
6.7(2)	**6.7(2)**	7.991(3)	510.3(3)
8.9(2)	**8.8(2)**	7.961(3)	504.5(3)
11.2(2)	**10.9(2)**	7.938(3)	500.2(3)
13.1(2)	**13.0(2)**	7.915(3)	495.8(3)
14.8(1)	**14.9(2)**	7.894(3)	492.0(4)
16.6(1)	**17.1(3)**	7.872(4)	487.8(4)
18.6(1)	**19.6(4)**	7.852(5)	484.1(5)
20.6(1)	**21.5(4)**	7.833(6)	480.7(6)
22.3(1)	**22.3(4)**	7.823(5)	478.8(6)
24.8(1)	**25.6(2)**	7.794(6)	473.5(6)
26.6(1)	**28.0(3)**	7.776(5)	470.1(5)
28.9(3)	**29.4(5)**	7.764(4)	468.0(4)

Note: The pressure values in bold are adopted for B-M EOS fittings.

hydrous ringwoodite. For the subsequent discussion, we adopt P_{ruby} for the first five pressure steps, and P_{neon} for the other steps of higher pressures. Such values are marked in bold in the table.

High-pressure powder diffraction data were collected at HP-CAT 16ID-B (λ = 0.3680 Å) on a MAR-CCD-X-ray detector and converted to 1D pattern using Fit2D (Hammersley et al. 1996). A single crystal was selected for optical clarity (no stishovite evident) and crushed gently between glass slides to avoid amorphization, and each sample loaded independently with Re gaskets in Ne at the GSECARS gas loading system (Rivers et al. 2008). Reported pressures are from the quasi-hydrostatic ruby fluorescence scale, calibrated using a He medium (Jacobsen et al. 2008). Pressures from the quasi-hydrostatic ruby fluorescence scale are similar to a stiffer argon pressure medium calibration (Mao et al. 1986) for the pressure range of the experiment, differing by less than 1.5% at 22 GPa. The consequences for the inferred equation of state are minor, with less than 1% difference in the bulk modulus for fixed K'. Pressures are also indistinguishable from neon diffraction where available (Hemley et al. 1989). Diffraction was collected in about 1 GPa steps upon compression to 19.4 GPa. Three to five diffraction patterns were collected at each pressure to monitor any development in pressure gradients and non-hydrostacity. The unit-cell parameters vs. pressures by powder diffraction are listed in Table 3.

X-ray diffraction for thermal expansion

The X-ray data of the sample at various temperatures were collected on a Bruker P4 four-circle diffractometer with a dual scintillation point detector system in the Mineral Physics and Crystallography Lab, Department of Geological Sciences, University of Colorado at Boulder. The size of the crystal was about 100 × 85 × 70 μm^3. The point system used an 18 KW rotating Mo-anode X-ray generator operated at 50 kV and 250 mA. Mo$K\alpha_1$–$K\alpha_2$ mixed characteristic wavelength was used, and $K\alpha$_avg of 0.71063 Å, calibrated by a spherical anhydrous forsterite single crystal, was used for unit-cell refinements. The temperature range was from

143 to 736 K: low-temperature experiments were controlled by an LT-2A controller using N_2 gas stream, whereas high-temperature measurements were conducted on a Bruker high-temperature device using two-prong ceramic-coated Pt wire radiant heating with an Omega temperature-control unit. See Ye et al. (2009) for details of the temperature calibration.

For each temperature step, the point-detector system was first used to refine the unit-cell parameters from 48 equivalent reflections of six unique reflections: (220), (311), (400), (422), (511), and (440). Subsequently, intensity scans were carried out on the point system to refine the internal structure. It took about 4 h for one complete scan, with 2θ scan range set to about 60°. In total, more than 300 reflections (51 unique reflections) were measured, except for 48 unique reflections at 489 K step and 53 unique reflections at 736 K step. Ye et al. (2009) reported the irreversible thermal expansion started at 606 K, and then the same processes of measurements were utilized to refine unit-cell parameters and internal structures at room temperature after heating to 635, 685, and 736 K, individually.

Refinements of atom positions and anisotropic displacement parameters were done using the program SHELXL-97 (Sheldrick 1997) in the software package WinGX (Farrugia 1999). We used scattering factors of Mg^{2+} and Si^{4+} cations from Cromer and Mann (1968), and those of O^{2-} anion by Tokonami (1965). In the refinements, Mg and Si cations are fixed at special positions of (½, ½, ½) and (1/8, 1/8, 1/8), respectively, and for the O anion: $x = y = z$. The occupancy of O was set to one (full), while the occupancies of Mg and Si (less than 1) were refined. Atom displacement parameters were refined anisotropically with $U_{11} = U_{22} = U_{33} = U_{ii}$, $U_{12} = U_{13} = U_{23} = U_{ij}$ for cubic structure ($U_{ij} << U_{ii}$ and $U_{eq} = U_{ii}$). The total numbers of reflections observed, R1, unit-cell parameters, fractional O coordinate (Xox) and occupancies are listed in Table 4, atomic anisotropic displacement parameters are listed in Table 5, and the bond lengths and polyhedral volumes calculated using XtalDraw (Downs et al. 1993) are listed in Table 6.

TABLE 3. Unit-cell parameters vs. pressure for powder XRD

P (GPa)	*a* (Å)	*V* (Å³)
2.4(1)	8.0472(4)	521.1(1)
2.9(1)	8.0335(9)	518.5(2)
3.6(1)	8.0251(5)	516.8(1)
4.6(1)	8.0054(9)	513.0(2)
5.4(1)	7.9963(7)	511.3(1)
6.2(1)	7.9888(5)	509.8(1)
7.0(1)	7.9799(5)	508.2(1)
7.6(1)	7.9758(6)	507.4(1)
8.4(1)	7.9590(4)	504.2(1)
9.3(1)	7.9504(6)	502.5(1)
10.3(1)	7.9352(4)	499.6(8)
11.3(1)	7.9273(5)	498.2(1)
12.3(2)	7.9108(6)	495.1(1)
13.4(2)	7.8993(5)	492.9(1)
14.7(2)	7.8861(8)	490.4(2)
15.6(2)	7.8720(5)	487.8(1)
16.4(2)	7.8660(7)	486.7(1)
17.6(2)	7.848(1)	483.3(2)
18.6(2)	7.8429(6)	482.4(1)
19.4(2)	7.8360(6)	481.2(1)

RESULTS AND DISCUSSION

Volume-hydration systematics

Panero (2010) reported a theoretical study of hydration mechanisms in ringwoodite. In addition to the unit-cell volumes and water contents, Figure 2 also shows the LDA-predicted volume-hydration trends for the three possible hydration mechanisms in ringwoodite. The anhydrous reference volume chosen in this study was from Sasaki et al. (1982), chosen because it was single crystal and because their sample showed the smallest volume among other reported anhydrous studies (e.g., Inoue et al. 2004; Jackson et al. 2000; Katsura et al. 2004; Akaogi et al. 1989). Relative to Sasaki et al. (1982), only the hydrous sample ringby4 from the study of Smyth et al. (2003) showed a smaller unit-cell volume. The next hydrous sample, containing about 0.2 wt% H_2O from Kudoh et al. (2007) has a similar value to that anhydrous reference reported by Sasaki et al. (1982). At all higher water contents, the cell volume increases significantly.

Between anhydrous samples and about 2 wt%, a single linear trend with a slope of 0.96(5) $Å^3/C_{H_2O}$ (where C_{H_2O} is the water concentration in wt% H_2O) was fitted (Fig. 2) that lies close to that predicted by LDA for $Mg^{2+} = 2H^+$ by Panero (2010). A second linear trend with slope of 3.3(2) $Å^3/C_{H_2O}$ was fitted to data with water contents above 2 wt% H_2O (Points 5, 6, 8, and 9 in Fig. 2), excluding the outlier (Point 7) from Wang et al. (2006), which we speculate contains a significantly higher concentration of defects other than $Mg^{2+} = 2H^+$ (or has a higher water content than reported).

Combining only SIMS water contents and Mg/Si ratios from electron microprobe data from the literature, a plot of that relationship is shown in Figure 3 and was used to estimate the Mg/Si ratio of the current sample, SZ0820, with Mg/Si = 1.9. The fitted trend to existing data (excluding SZ0820) shows a slope of about –0.039(7) Mg/Si per wt% H_2O, in excellent agreement with the GGA thermodynamic model of Panero (2010).

Using the literature data in Table 1 and new SIMS data for ringby2, ringby4, and SZ0820, we fit a single linear trend to the density of ringwoodite as a function of water content in Figure 4. The combined fitted equation is $\rho_0 = 3.564(5) - 0.049(3)\ C_{H_2O}$ (in g/cm³).

TABLE 4. Number of reflections, unit-cell parameters, and the occupancies of cations at different temperatures

T (K)	Total	R1 (%) / uniq. no. [Fo > 4σ(Fo)]*	*a* (Å)	*V* (Å³)	Xox	Mg occup.	Si occup.
143	276	4.05 / 47	8.0746(6)	526.46(7)	0.2437(2)	0.98(2)	1.00(3)
193	277	2.05 / 47	8.0756(6)	526.65(7)	0.2438(1)	0.97(2)	1.00(2)
243	276	1.80 / 46	8.0777(5)	527.06(6)	0.2438(1)	0.96(1)	0.98(2)
303	277	1.46 / 46	8.0816(4)	527.82(5)	0.2438(1)	0.95(1)	0.99(2)
350	274	2.77 / 43	8.0860(7)	528.69(7)	0.2437(2)	0.95(2)	1.00(2)
396	276	2.81 / 45	8.0889(5)	529.25(5)	0.2437(2)	0.96(2)	1.00(2)
443	277	2.35 / 45	8.0931(5)	530.08(6)	0.2438(2)	0.95(2)	1.00(2)
489	260	3.32 / 44	8.0976(5)	530.96(5)	0.2438(2)	0.96(2)	0.98(2)
537	275	3.32 / 43	8.1030(5)	532.04(6)	0.2437(2)	0.96(2)	1.00(2)
586	276	2.95 / 45	8.1084(7)	533.09(8)	0.2436(2)	0.94(2)	0.98(2)
635	273	4.39 / 47	8.1164(7)	534.68(8)	0.2437(2)	0.92(2)	0.95(2)
685	272	3.32 / 42	8.1279(8)	536.96(9)	0.2438(2)	0.94(2)	0.95(2)
736	288	4.12 / 45	8.1430(8)	539.94(9)	0.2438(2)	0.92(2)	0.93(2)
RT(635)†	273	2.45 / 46	8.0947(4)	530.41(5)	0.2440(2)	0.94(2)	0.96(2)
RT(685)	272	3.08 / 46	8.1031(4)	532.05(5)	0.2440(2)	0.93(2)	0.94(2)
RT(736)	271	4.33 / 44	8.1115(4)	533.70(4)	0.2442(2)	0.92(2)	0.91(2)

* R1 is the percentage for Fo > 4σ(Fo) with corresponding number of unique reflections listed behind "/."
† Measurement taken at room temperature after heating to 635 K.

TABLE 5. Anisotropic displacement parameters at various temperatures

	Mg		Si*	O	
T (K)	U_{ii}	U_{ij}	U_{ii}	U_{ii}	U_{ij}
143	0.0042(13)	–0.0006(4)	0.0061(15)	0.0039(14)	0.0007(6)
193	0.0049(8)	–0.0006(3)	0.0054(9)	0.0047(9)	0.0005(4)
243	0.0056(6)	–0.0005(2)	0.0052(7)	0.0059(7)	0.0006(3)
303	0.0058(6)	–0.0009(2)	0.0061(7)	0.0065(8)	0.0005(3)
350	0.0075(8)	–0.0007(4)	0.0083(9)	0.0081(11)	0.0007(5)
396	0.0081(9)	–0.0010(3)	0.0079(9)	0.0079(11)	0.0007(5)
443	0.0090(8)	–0.0010(3)	0.0088(9)	0.0089(10)	0.0004(4)
489	0.0104(11)	–0.0012(4)	0.0091(12)	0.0101(16)	–0.0002(6)
537	0.0109(10)	–0.0017(5)	0.0116(11)	0.0102(15)	0.0008(6)
586	0.0122(9)	–0.0016(4)	0.0121(9)	0.0132(14)	0.0008(5)
635	0.0127(12)	–0.0026(4)	0.0116(13)	0.0147(15)	0.0007(7)
685	0.0175(11)	–0.0024(4)	0.0160(11)	0.0180(16)	0.0004(7)
736	0.0205(12)	–0.0033(5)	0.0195(12)	0.0219(18)	0.0015(7)
RT(635)	0.0086(10)	–0.0013(4)	0.0100(11)	0.0095(14)	0.0008(6)
RT(685)	0.0110(9)	–0.0017(4)	0.0121(9)	0.0132(13)	0.0017(6)
RT(736)	0.0134(12)	–0.0022(4)	0.0142(13)	0.0168(15)	0.0019(8)

* For Si anisotropic refinement, U_{ij}= 0.

TABLE 6. Bond lengths and polyhedral volumes at temperatures

T (K)	Si–O (Å)	V(Si) (Å^3)	Mg–O (Å)	V(Mg) (Å^3)	V(non) (Å^3)
143	1.661(2)	2.351(6)	2.070(3)	11.791(17)	319.0(3)
193	1.662(1)	2.356(4)	2.070(3)	11.785(12)	319.2(2)
243	1.663(1)	2.358(3)	2.071(2)	11.793(9)	319.5(2)
303	1.663(1)	2.359(3)	2.072(2)	11.804(9)	320.1(2)
350	1.663(2)	2.359(5)	2.073(3)	11.842(15)	320.3(3)
396	1.663(2)	2.359(5)	2.075(3)	11.863(15)	320.6(3)
443	1.665(2)	2.368(5)	2.075(3)	11.867(15)	321.3(3)
489	1.666(2)	2.372(7)	2.076(4)	11.887(19)	321.8(3)
537	1.666(2)	2.372(6)	2.078(3)	11.923(18)	322.3(3)
586	1.666(2)	2.371(5)	2.080(3)	11.960(15)	322.8(3)
635	1.669(2)	2.384(6)	2.082(3)	11.982(18)	323.9(3)
685	1.672(2)	2.401(6)	2.084(3)	12.018(18)	325.5(3)
736	1.676(2)	2.417(7)	2.087(4)	12.080(19)	327.3(4)
RT(635)	1.669(2)	2.385(6)	2.073(3)	11.841(18)	321.9(3)
RT(685)	1.671(2)	2.393(5)	2.075(3)	11.878(15)	322.8(3)
RT(736)	1.675(2)	2.412(6)	2.076(3)	11.890(18)	324.2(3)

Compressibilities and seismic velocities

The third-order Birch-Murnaghan equation of state (B-M EOS) fitting using the program EOSFIT 5.2 (Angel 2001) gives values of V_0 = 529.5(5) Å^3, K_{T0} = 159(7) GPa, K' = 6.7(7) for single-crystal XRD; V_0 = 528.1(1) Å^3, K_{T0} = 161(4) GPa, K' = 5.4(6) for powder XRD. The calculated V_0 for single crystal is larger than that for powder, and also 0.32% larger than the value of 527.82(5) Å^3 measured at ambient condition in our lab. These discrepancies can be attributed the systematic difference between different experimental systems and conditions. Likewise, Ye et al. (2010) reported that hydrous wadsleyite had the V_0 value, by third-order B-M EOS for data collected also at GSECARS beamline 13 BM-D, 0.37% larger than that measured on Bruker P4 system. In addition, K_{T0} values for single crystal and powder have mutually overlapping uncertainties. However, the K' value from the single-crystal data set is larger than that from the powder data set, beyond the mutual uncertainties. These differences may reflect covariance between V_0 and K'.

Both compression data sets by single-crystal and powder diffraction are individually normalized to the calculated V_0 values above. V/V_0 vs. P are plotted in Figure 6, with third-order B-M EOS fitting curve for V/V_0 fixed to 1 at P = 0, and Birch normalized pressure (F_E) vs. Euler finite strain (f_E) is plotted in Figure 7, with the positive slope showing that K' is larger than 4. In addition, third-order B-M EOS fitting gives K_{T0} = 161.3(7) GPa for K' fixed at 6, and K_{T0} = 155.7(7) GPa for K' fixed at 7. All the results for third-order B-M EOS fitting are plotted in Figure 8 with confidence ellipsoids for 68.3, 90, and 95.4% (Angel 2000). The point for K' fixed at 6 is inside the ellipsoid of 68.3%, while the point for K' fixed at 7 is on the ellipsoid of 95.4%.

The isothermal compressibility studies by XRD for both anhydrous and hydrous ringwoodite are summarized in Table 7. Data in Table 7 demonstrate that K_{T0} decreases by about 12 GPa for every 1 wt% increase in water content, and increases about 1 GPa for every 10 mol% increase in fayalite content, indicating that the variation of H content has a much larger effect on bulk modulus than Fe content does within reasonable ranges of these parameters in Transition Zone (Smyth et al. 2004). These results are similar to those observed in wadsleyite by Ye et al. (2010) who concluded that K_{T0} of wadsleyite would also decrease 12 GPa for every 1 wt% increasing in water content. Hazen et al. (2000) reported K_{T0} of anhydrous Fo_{100} wadsleyite was 172(3) GPa, which was 6.5% smaller than anhydrous Fo_{100} ringwoodite (Hazen 1993). In addition, Holl et al. (2008) and Ye et al. (2010) reported that hydrous wadsleyite samples had K' values greater than 4 (but not bigger than 5) due the contribution from H^+ cations. Manghnani et al. (2005), Smyth et al. (2004), and the current study all show that K' values, refined by third-order B-M EOS, are greater than 6 for hydrous ringwoodite. Thus for ringwoodite, K' increases as water content increases, meaning that hydration makes it harder to compress the structure at higher pressure, and the large K' values for ringwoodite could be induced by the cubic-close-packed oxygen arrangement in the spinel structure (Manghnani et al. 2005).

The bulk sound speed is defined as $V_\varphi = (K_S/\rho)^{1/2}$, whereas K_S is adiabatic bulk modulus, and $K_S = K_T(1 + \alpha\gamma T)$, where K_T is isothermal bulk modulus, and α the thermal expansion coefficient. If we adopt the mean thermal expansion coefficient α_0 values from Ye et al. (2009) and Anderson-Gruneisen parameter from Meng et al. (1993), we can calculate the V_φ profiles from this study compared to those of previous studies. The densities and bulk sound speed vs. pressures are plotted in Figures 9a and 9b, respectively. Here for the curves of current study, we use V_0 = 527.82(5) Å^3 at ambient condition, K_{T0} = 160(2) GPa, and K' = 6.2(3). We extrapolate the pressure to 20 GPa, for the profiles of Hazen (1993), Ganskow et al. (2010), Smyth et al. (2004), and Yusa et al. (2000). Compared to Fo_{100} ringwoodite, every 10 mol% increase in fayalite content induces about 0.67% increase in unit-cell volume (Ganskow et al. 2010), 4.5% increasing in mol. mass, and about 3.8% increase in density. Every 1 wt% increase in H_2O would then cause about 1.4% decrease in density (Fig. 4). And the order of density curves in Figure 9a is consistent with the order of Fe contents. For Fo_{100} ringwoodite samples, the anhydrous one from Hazen (1993) has higher density than the hydrous ones from this study and Yusa et al. (2000). The density from Yusa et al. (2000) is slightly smaller than that from this study at ambient pressure, but an apparent crossover happens around 7 GPa, because K' from this study is 6.7(7), greater than K' of 5 (fixed) from Yusa et al. (2000). A greater K' leads to a lower compressibility at high pressure. From the above discussion, Fe increases density more significantly than bulk modulus, whereas H_2O could decrease bulk modulus more significantly than density. Hence, any increase in Fe or H_2O content would

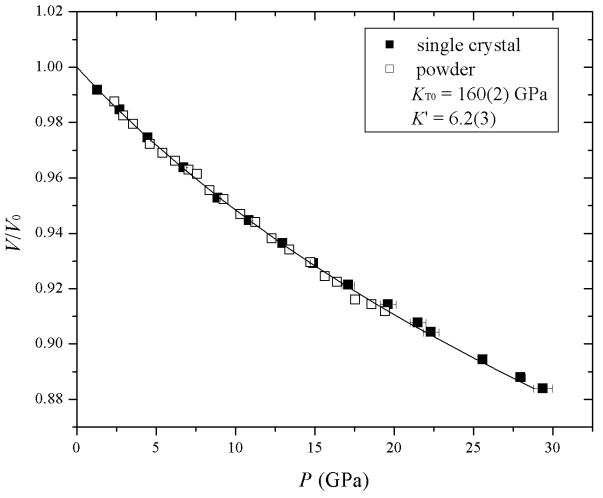

FIGURE 6. Normalized unit-cell volume (V/V_0) as a function of pressure (P). The fitting curve is third-order B-M EOS, with K_{T0} and K' values listed.

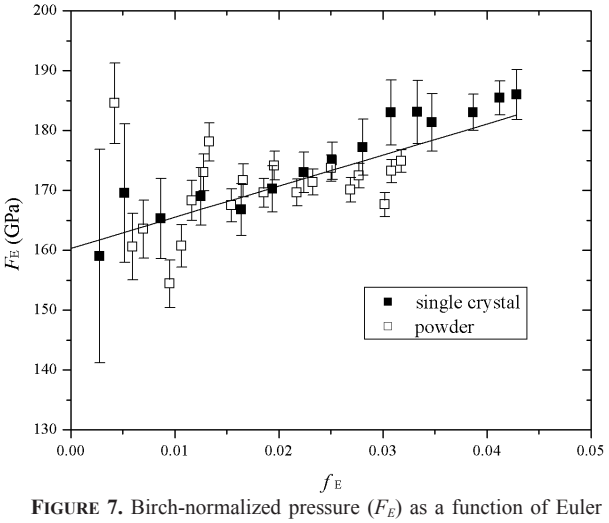

FIGURE 7. Birch-normalized pressure (F_E) as a function of Euler finite strain (f_E) plots with vertical error bars for the uncertainties of F_E. For $f_E > 0.02$ ($P > 11$ GPa), the plotted points for single crystal are systematically and significantly above the fitting line, while the points for powder are below the fitting line, because of larger K' for single crystal.

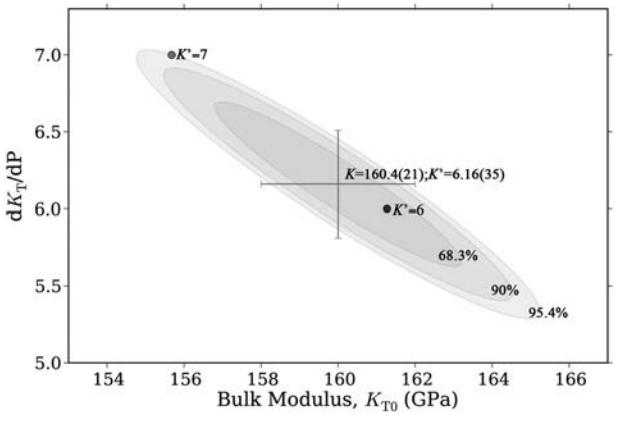

FIGURE 8. Confidence ellipsoid plots for K' vs. K_{T0} from third-order B-M EOS fittings.

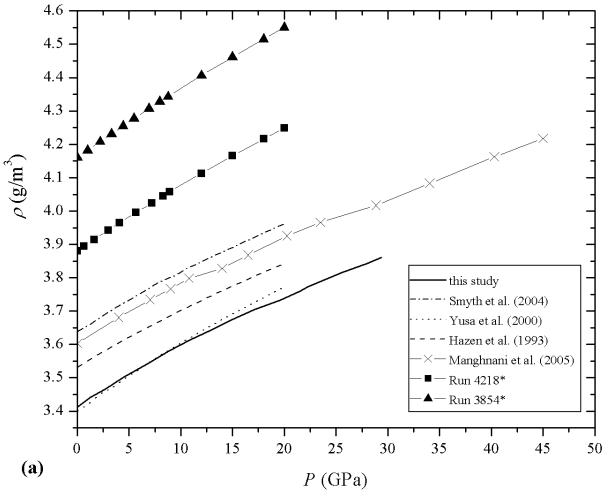

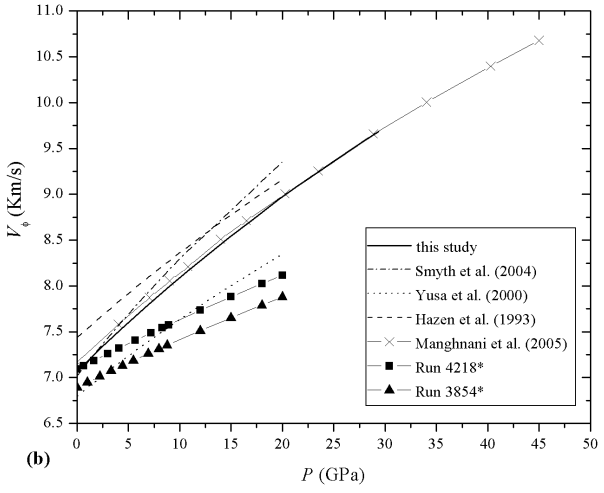

FIGURE 9. (**a** and **b**) profiles of density and bulk sound speed, respectively, for this study and literatures [* samples from Ganskow et al. (2010), and the sample from Hazen et al. (2000) is Fo_{100}]. The H_2O (wt%) and Fo (%) are 0, 100 for Hazen et al. (1993); 0.4, 61 for run 4218 of Ganskow et al. (2010); 0.7, 49 for run 3854 of Ganskow et al. (2010); 0.79, 88 for Manghnani et al. (2005); 0.93, 88 for Smyth et al. (2004); 2.6, 100 for current study; and 2.8, 100 for Yusa et al. (2000).

decrease the bulk sound velocity. This is consistent with the order of velocity curves in Figure 9b: run 3854 < run 4218 < Smyth et al. (2004) < Manghnani et al. (2005) for various Fe contents; Yusa et al. (2000) < this study < Hazen (1993) for different H_2O contents. Crossovers in velocity occur due to different K' values, and larger K' increase velocity more strongly at high pressures. However, the cross-derivatives of $d\alpha/dp$ have not been reported for hydrous ringwoodite samples.

In addition, anhydrous Fo_{100} ringwoodite has an adiabatic bulk modulus (K_{S0}) of about 185 GPa, and a shear modulus (μ_0) of about 120 GPa (Jackson et al. 2000; Weidner et al. 1984; Li 2003), and Sinogeikin et al. (2003) reported K_{S0} of 188(3) GPa, and μ_0 of 119(2) GPa for anhydrous Fo_{91} ringwoodite. Fo_{88} ringwoodite with about 1 wt% H_2O has K_{S0} of about 177 GPa, and μ_0 of about 103 GPa (Jacobsen et al. 2004; Jacobsen and Smyth 2006); Fo_{100} ringwoodite with about 2.2 wt% H_2O has K_{S0} of

TABLE 7. Isothermal compressibility parameters from XRD

H_2O (wt%)	Fo	V_0 (Å^3)	K_{T0} (GPa)	K′	P_{max} (GPa)	Reference
0	100	526.54(13)*	184(2)	4.8†	5	Hazen (1993)
0	40	546.61(14)*	203(2)	4.8†	5	Hazen (1993)
0	20	552.89(19)*	205(2)	4.8†	5	Hazen (1993)
0	0	558.80(14)*	207(2)	4.8†	5	Hazen (1993)
0.4	61	539.01(5)	184.1(7)	4†	8.9	run 4218 of Ganskow et al. (2010)
0.7	49	543.32(7)	186.5(9)	4†	8.8	run 3854 of Ganskow et al. (2010)
0.79	89	530.49(7)	175(3)	6.2(6)	45	Manghnani et al. (2005)
0.93	88	530.2(5)	169(3)	7.9(9)	11.2	Smyth et al. (2004)
2.5(3)	100	529.5(5)	159(7)	6.7(7)	29.4	This study (single-crystal)
528.1(1)	161(4)	5.4(6)	19.4			This study (powder)
160(2)	6.2(3)					This study (combined)
161.3(7)	6†					
155.7(7)	7†					
2.8	100	529.1(2)	148(1)	5†	5.9	Yusa et al. (2000)

* V_0 values are from measurements, while other V_0 values are calculated by B-M EOS fitting.
† K′ values are fixed.

approximately 160 GPa, and μ_0 of about 107 GPa (Wang et al. 2003; Inoue et al. 1998). Anhydrous ringwoodite samples have higher K_{S0} and μ_0 than hydrous ringwoodite samples, causing a decrease in both V_P and V_S at low pressures. Conversely, Jacobsen and Smyth (2006) reported $K' = 5.3$, $\mu' = 2.0$ for hydrous Fo_{100}; Li (2003) reported $K' = 4.5$, $\mu' = 1.5$ for anhydrous Fo_{100}; Sinogeikin et al. (2003) report $K' = 4.1$, $\mu' = 1.3$ for anhydrous Fo_{91}. Hydration could increase K' and μ', and then in return increase V_P and V_S more rapidly at high pressures (Jacobsen and Smyth 2006), similar to the effect on V_φ.

Thermal expansion study

Unit-cell volumes as a function of temperature for measurements at ambient pressures are plotted in Figure 10, with second-order polynomial fitting of the measured data up to 586 K as in Equation 1. From 638 K and above, the measured unit-cell volumes are significantly above the extrapolation of the fitting curve, consistent with irreversible expansion starting at about 606 K for this sample (Ye et al. 2009). The mean coefficient α_0 is $40(4)\times10^{-6}$/K (143–736 K), $29(2)\times10^{-6}$/K (143–586 K before irreversible expansion), and $35(1)\times10^{-6}$/K (303–586 K), which is exactly consistent with values reported by Ye et al. (2009), while 28% larger than the α_0 value for hydrous ringwoodite with 2.6 wt% H_2O from Inoue et al. (2004) by X-ray powder diffraction.

$$V\,(\text{Å}^3) = 2.1(2)\times10^{-5}\times T^2 + 0.001(1)\times T + 525.9(2). \quad (1)$$

In the ringwoodite unit cell, there are 8 Si^{4+} and 16 Mg^{2+} cations. Each Si^{4+} is coordinated with four O^{2-} anions forming a tetrahedron, and each Mg^{2+} cation is coordinated with six O^{2-} anions forming an octahedron. All oxygen atoms are equivalent and bonded to three Mg and one Si. Here we use V(Si) and V(Mg) to denote the tetrahedral and octahedral volumes, respectively, and define the non-polyhedral volume V(non) as in Equation 2 below

$$V(\text{non}) = V(\text{cell}) - 8\times V(\text{Si}) - 16\times V(\text{Mg}). \quad (2)$$

Fractional polyhedral volumes at various temperatures are plotted in Figure 11, normalized to the values at lowest experimental temperature of 143 K. V(Si) is found to expand significantly and abruptly above the onset of irreversible expansion at 586 K. The α_0 for V(Si) is $20(3)\times10^{-6}$/K (143–586 K), while a much larger value of $132(4)\times10^{-6}$/K (586–736 K).

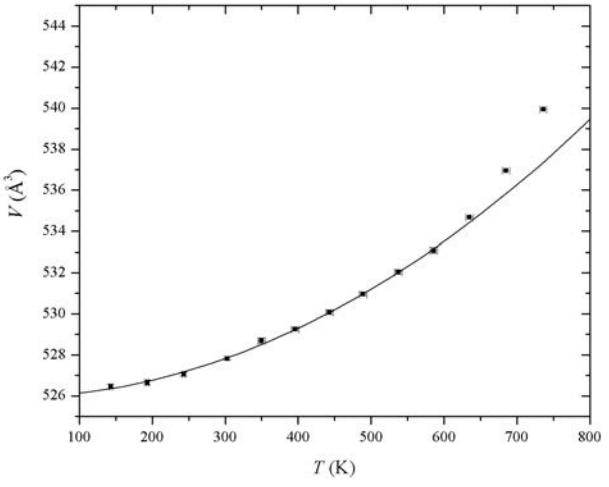

FIGURE 10. Cell volume (V) vs. temperature (T) plot with horizontal and vertical error bars for the uncertainties of T and V, respectively, if they are larger than the size of the symbols. Irreversible expansion starts at 635 K, the second-polynomial fitting curve ($R^2 = 0.9987$) is for the measured data blow 635 K.

However, such abrupt expansion is not observed for V(Mg) or V(non). Before the irreversible expansion, V(Si) has a smaller thermal expansion coefficient than V(Mg), which is consistent with the conclusion that V(Si) has less compressibility than that of V(Mg) (Smyth et al. 2004), because Si–O bond is shorter and stronger than Mg–O bond. Throughout the experimental temperature range (143–736 K), α_0 values for V(Mg) and V(non) are $41(3)\times10^{-6}$/K and $39(4)\times10^{-6}$/K, respectively, which are the same as that of unit-cell volume. In addition, intensity scans at room temperature after heating to 635 K show V(cell), V(Si), V(Mg), and V(non) expanded by 5, 11, 3, and 5%, respectively, compared with the initial volumes at room temperature; expanded by 8, 15, 6, and 8%, respectively, after heating to 685 K; expanded by 11, 22, 7, and 13%, respectively, after heating to 736 K. The room-temperature cell and polyhedral volumes expanded more after heating to higher temperatures, and the order of expansion is V(Mg) < V(cell) < V(Si). Hence, we can conclude that V(Si) expands most significantly during the disequilibrium irreversible expansion.

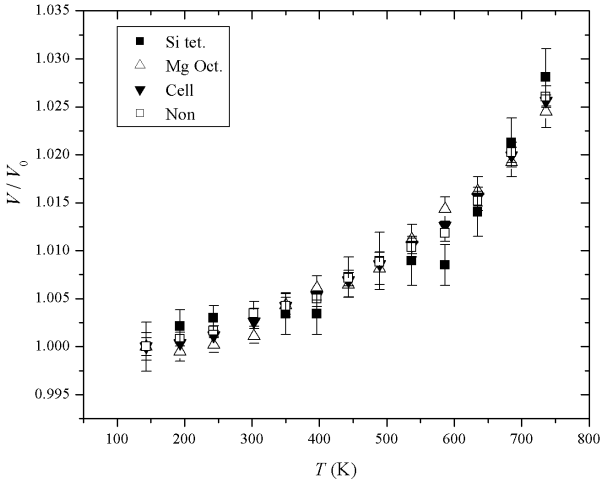

FIGURE 11. Fractional polyhedral volumes vs. *T*, normalized to the volumes at lowest experimental temperature of 143 K, with vertical error bars for the uncertainties of fractional volumes.

According to the ^{29}Si NMR spectroscopic study of hydrous ringwoodite from Stebbins et al. (2009b), the new NMR peaks, which cross-polarize very quickly, indicate very short Si-H distances and the presence of Si-OH, suggesting most of H^+ cations substitute into Mg^{2+} vacancies. In the hydrous ringwoodite structure, a small amount of H^+ would substitute into Si^{4+} vacancies as well, causing the occupancy of Si^{4+} to be slightly smaller than 1, but still greater than that of Mg^{2+} (Panero 2010). In Table 4 Si^{4+} occupancies at 635, 685, 736 K, and room temperature after heating, are significantly less than those before irreversible expansion, with the uncertainties taken into consideration. This suggests that a small amount of H^+ cations (less than 10%, estimated from the results of occupancies), initially in Mg^{2+} vacancies, might migrate and substitute Si^{4+} cations during irreversible thermal expansion, causing Si^{4+} occupancy to be smaller at room temperature after heating, compared with that at initial room temperature, i.e., the substituted Si^{4+} could not "go back" to the tetrahedral site after cooling. Maybe the transferring of H^+ cations from Mg^{2+} sites to Si^{4+} sites induces the abrupt increasing in V(Si). In contrast, only O1 atoms are protonated in hydrous wadsleyite structure without forming significant amounts of Si-OH groups (Stebbins et al. 2009b). Ye et al. (2011) report the cell volume of hydrous wadsleyite (2.8 wt% H_2O) decreased above 635 K due to dehydration, with 3 and 2.5% decreases in M2–O1 and M3–O1 bond lengths, respectively, but no significant change in V(Si), as opposed to the irreversible expansion observed in ringwoodite.

Furthermore, $F_{obs} - F_{cal}$ difference syntheses indicate a significant electron density peak at (½, ½, 0), 1.76 Å away from original Si site, from intensity data at 736 K, as well as room temperature after heating to 635, 685, and 736 K. This is an octahedral site with a cation-oxygen distance of about 1.95 Å. Therefore, if the irreversible transition is a consequence of H^+ substituting for Si^{4+}, then the Si^{4+} migrates to (½, ½, 0). We term this new octahedral site Si2, which is treated isotropically with U_{eq}(Si2) = U_{ii}(Si1), and again U_{ij}(Si1) = 0. The detailed results are listed in Table 8. The sum of Si1 and Si2 occupancies is consistent with that of Si in the first refinement in Table 4. Si2 occupancy increases slightly after heating to higher temperature, but is still no more than 0.05, compared with Si1 occupancy. R1 values are smaller in the second refinements than those in the first ones, and again V(Si1) expands more significantly than V(Mg) after heating above the irreversible expansion temperature. These results further support the speculation about the changes of polyhedral volumes during irreversible expansion. In the future, a ^{29}Si NMR spectroscopic study of hydrous ringwoodite after heating above 600 K might be able to confirm the presence of Si^{4+} at the (½, ½, 0) octahedral site.

TABLE 8. Second structure refinements for hydrous ringwoodite at room temperature after heating above 600 K with adding Si2 position

	RT(635)	RT(685)	RT(736)
R1 [Fo > 4σ(Fo)]	2.42	2.48	3.20
Xox	0.2441(2)	0.2442(2)	0.2444(2)
Mg occup.	0.94(2)	0.92(2)	0.90(2)
Si1 / Si2 occup.	0.95(3) / 0.01(2)	0.92(2) / 0.03(1)	0.87(2) / 0.05(1)
Mg (U_{ii} / U_{ij})	0.0086(10) / –0.0012(4)	0.0114(9) / –0.0017(3	0.0142(9) / –0.0021(3)
Si (U_{ii})	0.0100(11)	0.0124(9)	0.0147(10)
O (U_{ii} / U_{ij})	0.0098(14) / 0.0008(6)	0.0137(11) / 0.0017(6)	0.0176(10) / 0.0019(6)
V(Mg)*	1.003(2)	1.005(1)	1.005(2)
V(Si1)*	1.012(3)	1.017(2)	1.027(3)
V(non)*	1.006(1)	1.009(1)	1.014(1)

* The fractional polyhedral volumes normalized to those at initial room temperature.

ACKNOWLEDGMENTS

This work was supported by U.S. National Science Foundation grant EAR 07-11165 and 11-13369 to J.R.S., 09-55647 to W.R.P., 07-48707 to S.D.J., and by the David and Lucile Packard Foundation to S.D.J. Y.Y.C. acknowledges support from the Carnegie/DOE Alliance Center. The high-pressure single-crystal XRD portion of this work was performed at GeoSoilEnviroCARS (Sector 13), Advanced Photon Source (APS), Argonne National Laboratory. GeoSoilEnviroCARS is supported by the National Science Foundation, Earth Sciences (EAR-0622171) and Department of Energy, Geosciences (DE-FG02-94ER14466). The powder XRD portion of this work was performed at HPCAT (Sector 16), APS. HPCAT is supported by DOE-NNSA, DOE-BES, NSF, and the W.M. Keck Foundation. Use of the Advanced Photon Source was supported by DOE-BES, under contract no. DE-AC02-06CH11357.

REFERENCES CITED

Akaogi, M., Ito, E., and Navrotsky, A. (1989) The olivine-modified spinel-spinel transitions in the system Mg_2SiO_4–Fe_2SiO_4: Calorimetric measurements, thermochemical calculation, and geophysical application. Journal of Geophysical Research, 94, 15671–15685.

Anderson, D.L. (2007) New Theory of the Earth. Cambridge University Press, U.K.

Angel, R.J. (2000) Equations of state. In R.M. Hazen and R.T. Downs, Eds., High-pressure and High-temperature Crystal Chemistry, 41, p. 35–60. Reviews in Mineralogy and Geochemistry, Mineralogical Society of America, Chantilly, Virginia.

——— (2001) EoSFit, a program for fitting equations of state to *P-K-T* data. Version 5.2. Crystallography Laboratory, Virginia Tech, Blacksburg.

Cromer, D.T. and Mann, J. (1968) X-ray scattering factors computed from numerical Hartree-Fock wave functions. Acta Crystallographica, A24, 321–325.

Dera, P. (2007a) GSE-ADA data analysis program for monochromatic single crystal diffraction with area detector. GeoSoilEnviroCARS, Argonne, Illinois.

——— (2007b) RSV reciprocal space viewer program for single crystal data analysis. GeoSoilEnviroCARS, Argonne, Illinois.

Dorogokupets, P.I. and Dewaele, A. (2007) Equations of state of MgO, Au, Pt, NaCl-B1 and NaCl-B2: Internally consistent high-temperature pressure scales. High Pressure Research, 27, 431–436.

Downs, R.T., Bartelmehs, K.L., Gibbs, G.V., and Boisen, M.B. (1993) Interactive software for calculating and displaying X-ray or neutron powder diffractometer patterns of crystalline materials. American Mineralogist, 78, 1104–1107.

Farrugia, L.J. (1999) WinGX software package. Journal of Applied Crystallography, 32, 837–838.

Fei, Y., Ricolleau, A., Frank, M., Mibe, K., Shen, G., and Prakapenka, V. (2007) Toward an internally consistent pressure scale. Proceedings of the National

Academy of Sciences, 104, 9182–9186.
Ganskow, G., Ballaran, T.B., and Langenhorst, F. (2010) Effect of iron on the compressibility of hydrous ringwoodite. American Mineralogist, 95, 747–753.
Hammersley, A.P., Svensson, S.O., Hanfland, M., Fitch, A.N., and Häusermann, D. (1996) Two-dimensional detector software: From real detector to idealised image or two-theta scan. High Pressure Research, 14, 235–248.
Hazen, R.M. (1993) Comparative compressibilities of silicate spinels: anomalous behavior of (Mg, Fe)$_2$SiO$_4$. Science, 259, 206–209.
Hazen, R.M., Weinberger, M.B., Yang, H., and Prewitt, C.T. (2000) Comparative high-pressure crystal chemistry of wadsleyite, β-(Mg$_{1-x}$Fe$_x$)$_2$SiO$_4$, with x = 0 and 0.25. American Mineralogist, 85, 770–777.
Hemley, R.J., Zha, C.S., Jephcoat, A.P., Mao, H.K., and Finger, L.W. (1989) X-ray diffraction and equation of state of solid neon to 110 GPa. Physical Review B, 39, 11820–11827.
Holl, C.M., Smyth, J.R., Jacobsen, S.D., and Frost, D.J. (2008) Effects of hydration on the structure and compressibility of wadsleyite, β-(Mg$_2$SiO$_4$). American Mineralogist, 93, 598–607.
Inoue, T., Weidner, D.J., Northrup, P.A., and Parise, J.B. (1998) Elastic properties of hydrous ringwoodite (γ-phase) in Mg$_2$SiO$_4$. Earth and Planetary Science Letters, 160, 107–113.
Inoue, T., Tanimoto, Y., Irifune, T., Suzuki, T., Fukui, H., and Ohtaka, O. (2004) Thermal expansion of wadsleyite, ringwoodite, hydrous wadsleyite and hydrous ringwoodite. Physics of the Earth and Planetary Interiors, 143–144, 279–290.
Ito, E. and Katsura, T. (1989) A temperature profile of the mantle transition zone. Geophysical Research Letters, 16, 425–428.
Jackson, J.M., Sinogeikin, S.V., and Bass, J.D. (2000) sound velocities and elastic properties of γ-Mg$_2$SiO$_4$ to 873 K by Brillouin spectroscopy. American Mineralogist, 85, 296–303.
Jacobsen, S.D. and Smyth, J.R. (2006) Effect of water on the sound velocities of ringwoodite in the transition zone. In S.D. Jacobsen and S. Van der Lee, Eds., Earth's Deep Water Cycle, 168, p. 131–145. Geophysical Monograph, American Geophysical Union, Washington, D.C.
Jacobsen, S.D., Smyth, J.R., Spetzler, H., Holl, C.M., and Frost, D.J. (2004) Sound velocities and elastic constants of iron-bearing hydrous ringwoodite. Physics of the Earth and Planetary Interiors, 143–144, 47–56.
Jacobsen, S.D., Holl, C.M., Adams, K.A., Fischer, R.A., Martin, E.S., Bina, C.R., Lin, J.F., Prakapenka, V.B., Kubo, A., and Dera, P. (2008) Compression of single-crystal magnesium oxide to 118 GPa and a ruby pressure gauge for helium pressure media. American Mineralogist, 93, 1823–1828.
Katsura, T., Yokoshi, S., Song, M., Kawabe, K., Tsujimura, T., Kubo, A., Ito, E., Tange, Y., Tomioka, N., Saito, K., Nozawa, A., and Funakoshi, K. (2004) Thermal expansion of Mg$_2$SiO$_4$ ringwoodite at high pressures. Journal of Geophysical Research, 109, B12209, DOI: 10.1029/2004JB003094.
Koch-Müller, M. and Rhede, D. (2010) IR absorption coefficients for water in nominally anhydrous high-pressure minerals. American Mineralogist, 95, 770–775.
Kohlstedt, D.L., Keppler, H., and Rubie, D.C. (1996) Solubility of water in the α, β, and γ phases of (Mg,Fe)$_2$SiO$_4$. Contributions to Mineralogy and Petrology, 123, 345–357.
Kudoh, Y., Kuribayashi, T., Mizobata, H., and Ohtani, E. (2000) Structure and cation disorder of hydrous ringwoodite, γ-Mg$_{1.89}$Si$_{0.98}$H$_{0.30}$O$_4$. Physics and Chemistry of Minerals, 27, 474–479.
Kudoh, Y., Kuribayashi, T., Mizobata, H., Ohtani, E., Sasaki, S., and Tanaka, M. (2007) Pressure dependence of *u* parameter in ringwoodite up to 7.9 GPa. Journal of Mineralogical and Petrological Sciences, 102, 8–11.
Li, B. (2003) Compressional and shear wave velocities of ringwoodite γ-Mg$_2$SiO$_4$ to 12 GPa. American Mineralogist, 88, 1312–1317.
Libowitzky, E. and Rossman, G.R. (1997) An IR absorption calibration for water in minerals. American Mineralogist, 82, 1111–1115.
Manghnani, M.H., Amulele, G., Smyth, J.R., Holl, C.M., Shen, G., and Prakapenka, V. (2005) Equation of state of hydrous Fo90 ringwoodite to 45 GPa by synchrotron powder diffraction. Mineralogical Magazine, 69, 317–324.
Mao, H.K., Xu, J., and Bell, P.M. (1986) Calibration of the ruby pressure gauge to 800 kbar under quasi-hydrostatic conditions. Journal of Geophysical Research, 91, 4673–4676.
Meng, Y., Weidner, D.J., Gwanmesia, G.D., Liebermann, R.C., Vaughan, M.T., Wang, Y., Leinenweber, K., Pacalo, R.E., Yeganeh-Haeri, A., and Zhao, Y. (1993) In Situ high *P*-*T* X-ray diffraction studies on three polymorphs (α, β, γ) of Mg$_2$SiO$_4$. Journal of Geophysical Research, 98, 22199–22207.
Panero, W.R. (2010) First principles determination of the structure and elasticity of hydrous ringwoodite. Journal of Geophysical Research, 115, B03203, DOI: 10.1029/2008JB006282.
Ringwood, A.E. (1966) The chemical compositions and origin of the earth. In P.M. Hurley, Ed., Advances in the Earth Science, p. 287–356. M.I.T. Press, Cambridge, Massachusetts.
Rivers, M., Prakapenka, V.B., Kubo, A., Pullins, C., Holl, C.M., and Jacobsen, S.D. (2008) The COMPRES/GSECARS gas-loading system for diamond anvil cells at the Advanced Photon Source. High Pressure Research, 28, 273–292.
Sasaki, S., Prewitt, C.T., Sato, Y., and Ito, E. (1982) Single-crystal X-ray study of gamma Mg$_2$SiO$_4$. Journal of Geophysical Research, 87(B9), 7829–7832.
Sheldrick, G.M. (1997) SHELXL97, Release 97-2. Program for the refinement of crystal structures. University of Göttingen, Germany.
Sinogeikin, S.V., Bass, J.D., and Katsura, T. (2003) Single-crystal elasticity of ringwoodite to high pressures and high temperatures: Implications for 520 km seismic discontinuity. Physics of the Earth and Planetary Interiors, 136, 41–66.
Smyth, J.R., Holl, C.M., Frost, D.J., Jacobsen, S.D., Langenhorst, F., and McCammon, C.A. (2003) Structural systematics of hydrous ringwoodite and water in the Earth's interior. American Mineralogist, 88, 1402–1407.
Smyth, J.R., Holl, C.M., Frost, D.J., and Jacobsen, S.D. (2004) High pressure crystal chemistry of hydrous ringwoodite and water in the Earth's interior. Physics of the Earth and Planetary Interiors, 143–144, 271–278, DOI: 10.1016/j.pepi.2003.08.011.
Stebbins, J.F., Panero, W.R., Smyth, J.R., and Frost, D.J. (2009a) Forsterite, wadsleyite and ringwoodite: ^{29}Si NMR constraints on structural disorder and effects of paramagnetic impurity ions. American Mineralogist, 94, 626–629.
——— (2009b) Forsterite, hydrous and anhydrous wadsleyite and ringwoodite (Mg$_2$SiO$_4$): ^{29}Si NMR results for chemical shift anisotropy, spin-lattice relaxation, and mechanism of hydration. American Mineralogist, 94, 905–915.
Tokonami, M. (1965) Atomic scattering factor for O^{2-}. Acta Crystallographica, 19, 486.
Wang, J., Sinogeikin, S.V., Inoue, T., and Bass, J.D. (2003) Elastic properties of hydrous ringwoodite. American Mineralogist, 88, 1608–1611.
——— (2006) Elastic properties of hydrous ringwoodite at high-pressure conditions. Geophysical Research Letters, 33, L14308, DOI: 10.1029/2006GL026441.
Weidner, D.J., Sawamoto, H., Sasaki, S., and Kumazawa, M. (1984) Single-crystal elastic properties of the spinel phase of Mg$_2$SiO$_4$. Journal of Geophysical Research, 89, 7852–7860.
Ye, Y., Schwering, R.A., and Smyth, J.R. (2009) Effects of hydration on thermal expansion of forsterite, wadsleyite, and ringwoodite at ambient pressure. American Mineralogist, 94, 899–904.
Ye, Y., Smyth, J.R., Hushur, A., Manghnani, M.H., Lonappan, D., Dera, P., and Frost, D.J. (2010) Crystal structure of hydrous wadsleyite with 2.8% H$_2$O and compressibility to 60 GPa. American Mineralogist, 95, 1765–1772.
Ye, Y., Smyth, J.R., and Frost, D.J. (2011) Structural study of the coherent dehydration of wadsleyite. American Mineralogist, 96, 1760–1767.
Yusa, H., Inoue, T., and Ohishi, Y. (2000) Isothermal compressibility of hydrous ringwoodite and its relation to the mantle discontinuities. Geophysical Research Letters, 27, 413–416.

Manuscript received September 23, 2011
Manuscript accepted December 3, 2011
Manuscript handled by Lars Ehm